lator, consisting of a resistojet size nozzle which would simulate a thruster plume, was not attached to the thrust stand. Cell pressure P was varied by adding nitrogen gas (GN_2) away from the thrust stand to minimize its spouting velocity effect on winds in the cell. Propellant flow was introduced through the simulator while propellant to the thruster was turned off. Figure 2a presents a reference calibration to show the effect of P without simulator flow on the thrust readings. These data indicate that the thrust stand is relatively unaffected (less than 0.01 g) by the test chamber gases until $P \simeq 300\ \mu$ is reached. Thereafter, an increasingly strong positive force is indicated as P in increased. This is a facility-pumping-system-induced phenomenon, and it occurred in all data taken. (The "no simulator flow" calibration was repeated using hydrogen to vary cell pressure with similar results.)

Figures 2b and 2c show the results of typical resistojet flows using H_2 and NH_3 with the simulator. A significant negative force is observed for $P < 100\ \mu$. The windage force curves are similar for both propellants reaching maximum negative values of about 0.1 g. The maximum negative force for NH_3 occurs at a lower P than for H_2. The windage forces can be converted to effective specific impulse (I_{sp}) reduction by dividing by the mass flow rate. Thus, for the 0.1-g maximum negative force, corresponding I_{sp} reductions are 13 and 6.2 sec, respectively, for H_2 and NH_3 propellants. The windage force is repeatable for a given set of thruster/thrust-stand/test-chamber characteristics and for a given method of introducing bleed gas and given pumping station characteristics. It must be redetermined if any of these factors are changed.

Figures 3a and 3b present data for a range of cell pressure of three orders of magnitude for H_2 and NH_3 propellants, respectively. These data have been corrected for windage effects. Mass flow rate is constant in each case, and maximum specific I_{sp} corresponds closely to the design thrust of 10 mlb. These data indicate typical life-test conditions with respect to power and mass flow rate conditions but are not to be interpreted as thruster maximum capability.

In Fig. 3c the solid lines correspond to mean fits to the data in Figs. 3a and 3b. Note that different ordinate scales are used for hydrogen and ammonia propellant cases. Dotted lines are introduced to show a cell pressure times nozzle exit area (PA) force correction. The final curves corrected for windage and PA forces represent what can be termed a viscous-nozzle effect.

The magnitude of the three cell pressure effects (windage, PA force, and viscous-nozzle) of Fig. 3c are tabulated in Table 2. The percentage effects of these forces on hard-vacuum (0.5 μ) specific impulse are also tabulated. As evidenced by these data, the windage and PA force are second-order compared to the viscous-nozzle effect.

Post-Life-Test Performance

Several high-temperature performance runs were made on the B-2 thruster in the high-vacuum facility and are described in Table 3. These data were obtained after the B-2 thruster had been life-tested in excess of 6000 hr (more than 6000 duty cycles). For comparison, the life-test data of Ref. 2 indicated over-all total power efficiencies as follows: 1) 51% at 640-sec specific impulse on hydrogen propellant, and 2) 42% at 320-sec specific impulse on ammonia propellant. These values correspond to life-test cell pressures for which a cell-pressure penalty occurred. A significant improvement in efficiency as a result of the lower P is reflected in the Table 3 values.

Table 3 B-2 thruster high-vacuum cell performance

Propellant	Thrust, g	Specific impulse, sec	Electric power, w	Over-all-total power efficiency[a]
H_2	4.48	634	180	0.65
H_2	4.60	669	221	0.59
H_2	4.85	686	227	0.62
H_2	5.85	625	235	0.64
NH_3	4.42	320	141	0.45
NH_3	5.23	326	169	0.46

[a] Over-all total power efficiency: $\eta \triangleq$ (thrust) × (specific impulse)/20.8 × (total power) where total power is the sum of the initial power in the propellant gas and the applied electric power.

Specific impulse of the resistojet is an indication of the chamber gas temperature entering the thruster nozzle. The Table 3 data suggest chamber temperatures ranging from 1700° to 2100°K for hydrogen and about 1900°K for ammonia. Metallographic examinations of the heating elements of the life tested thrusters show[2] that an adverse temperature distribution existed in the concentric tubes heater. Gas flow suffered an actual cooling effect in the last heater passage. Structural temperatures had to be higher for a given I_{sp} than they would had the temperature gradient been favorable. The adverse temperature distribution results in a lower efficiency and higher power consumption than for the same I_{sp} in a thruster with a favorable distribution.

An improved resistojet, currently under development, has a contoured heater element which will give a more favorable temperature distribution, thereby permitting higher I_{sp} and efficiency for a given limit on maximum structural temperature. For a maximum structural temperature of 2400°K, we predict 66% efficiency at 700-sec specific impulse for hydrogen and 50% efficiency at 340 sec for NH_3.

References

[1] Halbach, C. R. and Yoshida, R. Y., "Development of a Biowaste Resistojet," AIAA Paper 70-1133, Stanford, Calif., 1970.
[2] Yoshida, R. Y. et al. "Resistojet Thruster Life Tests and High Vacuum Performance," Rept. CR-66970, 1970, NASA.

Spacer Effects on Lateral Heat Transfer in Multilayer Insulation

P. S. JAGANNATHAN* AND C. L. TIEN†
University of California, Berkeley, Calif.

LATERAL heat transfer plays an important role in the thermal performance of multilayer insulation systems.[1,2] For the case of an ideal dielectric (i.e., nonabsorbing and nonscattering) theoretical results agree well with the reported experimental data.[3] The spacers used in practice such as Dexiglas, Tissuglas, and others are, however, highly scattering and absorbing. Approximating them to ideal dielectrics may involve appreciable errors. This Note seeks an approximate analytical solution for the spacer effects. Special emphasis is placed on arriving at a solution which would make full use of the existing solutions for the case of nonabsorbing and nonscattering spacers.

Analysis

The system consists of two parallel conducting and radiating plates of finite length L and infinite width. The ends

Presented as Paper 70-849 at the AIAA 5th Thermophysics Conference, Los Angeles, Calif., June 29–July 1, 1970; submitted August 26, 1970; revision received October 16, 1970. Work supported by NASA Lewis Research Center under grant NGR-05-003-285.

* Department of Mechanical Engineering.
† Professor and Chairman, Department of Mechanical Engineering. Associate Fellow AIAA.

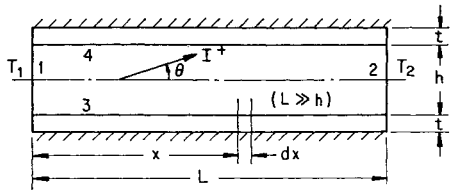

Fig. 1 Schematic of the physical system ($I = I^+$ for $-\pi/2 < \theta < \pi/2$ and $I = I^-$ for $\pi/2 < \theta < 3\pi/2$).

are maintained at temperatures, T_1 and T_2 (Fig. 1). The two plates are separated by an absorbing and isotropically scattering dielectric, and $h \ll L$. Boundaries 1 and 2 are opaque. Boundaries 3 and 4 are gray diffuse emitters and specular reflectors, and are both externally insulated.

The analysis of the problem proceeds in a similar manner as in the case of ideal dielectric spacer,[3] except that the definition of conduction-radiation parameter N is slightly modified to take into account the absorbing characteristics of the spacer. In the present case,

$$N \equiv 2\sigma T_1^3 h^2 n^4/(n^2 + k^2)\kappa a t \tag{1}$$

where σ is the Stefan-Boltzmann constant, n and k the real and imaginary parts of the complex refractive index $(n - ik)$, κ the thermal conductivity of the plate, a the transmittance constant depending upon the surface reflectance, and t the plate thickness.

An expression for the variation of transmittance with lateral distance x is needed to determine a. The power transfer for the case of nonconducting walls per unit area of the source per unit difference in emissive powers is termed as the transmittance.[4] The starting point in formulating the equation for power transfer is to develop the expression for the intensity of radiation I within the medium.

An essential assumption in the present analysis is that the variation of intensity in the perpendicular direction has negligible effect on the lateral heat transfer. This is valid when $L \gg h$. The intensity at any section x is assumed to be given by that at the midpoint between the two plates at that section and is a function of nondimensionalized lateral distance $y(\equiv x/h)$ and the directional cosine μ, where $\mu = \cos\theta$, and θ is the polar angle. Since the walls are specular reflectors, the ray tracing technique[5] can be used, and the intensity at any section y is given as

$$I^+(y,\mu) = \frac{\sigma T_1^4}{\pi} \rho_\mu^{M(y,\mu)} e^{-\beta h y/\mu} + \beta h \int_0^y s(y') \rho_\mu^{M(y-y')/\mu} \frac{dy'}{\mu} \tag{2}$$

$$I^-(y,-\mu) = \frac{\sigma T_2^4}{\pi} \rho_\mu^{M(L_0-y,\mu)} e^{-\beta h(L_0-y)/\mu} + \beta h \int_y^{L_0} s(y') \rho_\mu^{M(y'-y,\mu)} e^{-\beta h(y'-y)/\mu} \frac{dy'}{\mu} \tag{3}$$

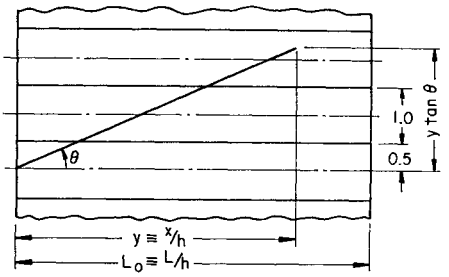

Fig. 2 Ray tracing for specular reflectors.

where $L_0 \equiv L/h$, β is the extinction coefficient, ρ_μ the surface reflectance for angle of incidence θ, $s(y')$ the source function and $M(y,\mu)$ the number of reflections for lateral distance y and angle θ given by (see Fig. 2).

$$M \equiv (\text{truncated integer})(|y \tan\theta| - 0.5) \tag{4}$$

From Eqs. (2) and (3) it is clear that the intensity at any section is given as the sum of two terms. The first term is the end intensity attenuated by the beam transmittance and the second is the result of contributions from all interior points attenuated by the line transmittance. The beam transmittance and the line transmittance are similar to those in the case of unidimensional gaseous radiation problem, except that the reflections on the side wall are also taken into account here. Hence, the problem reduces to that of unidimensional gaseous radiation, once the extinction coefficient is corrected for the reflections along the side walls. This correction is achieved through the following kernel-approximation formulas:

$$A \int_0^1 e^{-\beta_c h y/\mu}\, d\mu = \int_0^1 e^{-\beta h y/\mu} \rho_\mu^{M(y,\mu)}\, d\mu \tag{5}$$

$$A \int_0^1 e^{-\beta_c h y/\mu}\, \mu d\mu = \int_0^1 e^{-\beta h y/\pi} \rho_\mu^{M(y,\mu)}\, \mu d\mu \tag{6}$$

where A and β_c are constants determined from the above equations. The parameter β_c represents an extinction coefficient corrected for the presence of spacers. Similar kernel-approximation techniques have been widely used in radiative transfer problems.[5]

The concept of transmittance is meaningful only if it depends solely on the lateral distance and surface reflectance. This requirement is satisfied for unidimensional radiative transfer in a gray gas under radiative equilibrium.[5] Hence, the source function s is approximated by $n^4\sigma T^4/\pi(n^2 + k^2)$ which completes the analogy between unidimensional gray gas radiative equilibrium and the present system. The transmittance constant can be evaluated as $1.5\,\beta_c h$ on the basis of the exponential approximation employed for gray gas under radiative equilibrium.

Table 1 Physical parameters of various spacer materials

Spacer material	Absorption coefficient α, cm^{-1}	Scattering coefficient γ, cm^{-1}	Nominal thickness $h \times 10^3$, cm	Correction[a] factor $f \equiv (\beta_c - \beta)/\beta$	Radiation[b] to conduction parameter N	Optical[c] length parameter l	κ_e/κ[d]
Tissuglas[e]	3	265	25	0.004	0.006	4044	1.011
Dexiglas[e]	13	260	50	0.002	0.013	4110	1.024
Refrasil A100	<2	38	483	0.0013	0.804	600	2.507
Refrasil B100	<2	33	483	0.0015	0.918	525	2.722
Low-density foam	($\beta = \alpha + \gamma = 6 - 20$)		76–89	0.014–0.056	0.249–0.943	96–303	1.467–2.768

[a] For small f, an approximate estimate of f is given by $f = -\ln \rho/2\beta h$. The shield reflectance ρ is taken as 0.95.
[b] From Eq. (1) for $T_1 = 300°$K, $\kappa = 1.5$W/cm°K, $n = 1.4$, $k = 0$, $t = 4 \times 10^{-6}$ cm, and $a = 3\beta_c h/2$.
[c] $l = aL/h = 3\beta_c L/2$, L is taken as 10 cm.
[d] From Eq. (7) for $\theta_2 = (T_2/T_1) = 0.5$.
[e] In case of Tissuglas and Dexiglas the normal thicknesses of single layer are 1.5×10^{-3} cm and 7.6×10^{-3} cm, respectively. However normally several layers are used to keep the layer density within practical limits.

Results and Discussion

Calculations were carried out on some of the important spacer materials, namely Dexiglas (C. H. Dexter and Sons Paper Co.), Tissuglas (Pallflex Products Co.), silica fiber felt (called "refrasil," H. I. Thompson Co.)[6] and low-density foam (freon blown polyurethane with density $\approx$ 2 lbm/ft^3).[7] No reliable data for the extinction coefficient of these materials are available. The values used here are from Cunnington et al. for a source temperature of 500°K with an estimated experimental error of 50%. The results presented in Table 1 indicate that the correction on the extinction coefficient is negligible for these materials under normal values of spacer thickness and shield reflectance. This implies that the influence of wall reflections on the heat transfer is small compared to that due to spacer scattering.

It is also clear from Table 1 that the extinction coefficients of most of the spacer materials are large enough that the optically thick situation exists. The effective conductivity κ_e is given by

$$\kappa_e = \kappa + \kappa N(1 + \theta_2)(1 + \theta_2^2) \qquad (7)$$

where $\theta_2 \equiv T_2/T_1$. The first term on the right-hand side is the conduction contribution, while the second term represents the radiation contribution.

These calculations also reveal that under normal working conditions, radiation plays an insignificant role in the lateral heat transfer when Dexiglas or Tissuglas is used as spacers. The scattering is so large in these cases that it effectively localizes the radiation. These observations are borne out by the fact that theoretical predictions of Tien et al.[8] on the basis of purely conductive heat transfer with size effect agree well with the data of Coston and Vliet.[3] In the case of silica fiber felt or low-density foam spacer systems, substantial contribution to the lateral heat transfer from radiation is expected. However, there are no data available to check the validity of these predictions. It should be emphasized here that the above calculations are based on the assumption that the gap spacing is completed filled with the space material. For loosely packed spacers as in most applications a greater contribution of radiation than predicated is expected .[10]

Pogson and MacGregor[11] have analyzed the problem of selective slitting of individual layers to increase the thermal resistance due to conduction. This will have an effect of increasing the percentage of radiative contribution to the total heat transfer; however, the two-dimensional heat conduction in the layer renders the radiation-conduction interaction problem a complicated two-dimensional one. Further experimental and theoretical studies on the two-dimensional radiation-conduction interaction are needed.

References

[1] Vliet, G. C. and Coston, R. M., "Thermal Energy Transport Parallel to the Laminations in Multilayer Insulation," *Advances in Cryogenic Engineering*, Vol. 13, 1968, pp. 671–679.

[2] Androulakis, J. G. and Kosson, R. M., "Effective Thermal Conductivity Parallel to the Laminations and Total Conductance for Combined Parallel and Normal Heat Flow in Multilayer Insulation," *Journal of Spacecraft and Rockets*, Vol. 6, No. 7, July 1969, pp. 841–845.

[3] Tien, C. L., Jagannathan, P. S., and Armaly, B. F., "Analysis of Lateral Conduction and Radiation Along Two Parallel Long Plates," *AIAA Journal*, Vol. 7, No. 9, Sept. 1969, pp. 1806–1808.

[4] Edwards, D. K. and Tobin, R. D., "Effect of Polarization on Radiant Heat Transfer Through Long Passages," *Journal of Heat Transfer*, Vol. 89C, 1967, pp. 132–138.

[5] Sparrow, E. M. and Cess, R. D., *Radiation Heat Transfer*, Brooks/Cole, Belmont, Calif., 1967.

[6] Cunnington, G. R. et al., "Performance of Multilayer Insulation Systems for Temperature to 700°K," CR-907, 1967, NASA.

[7] Cunnington, G. R., private communication, Lockheed Research Lab., Palo Alto, Calif., 1970.

[8] Tien, C. L. et al., "Thermal Conductivity of Thin Metallic Films and Wires at Cryogenic Temperatures," *Proceedings of Eighth Thermal Conductivity Conference*, Plenum Press, New York, 1969, pp. 13–20.

[9] Coston, R. M. and Vliet, G. C., "Thermal Energy Transport Characteristics Along the Laminations of Multilayer Insulations," *Thermophysics of Spacecraft and Planetary Bodies*, Academic Press, New York, 1968, pp. 909–923.

[10] Jagannathan, P. S., "Lateral Heat Transfer in Multilayer Insulation," Ph.D. thesis, Jan. 1971, Univ. of California.

[11] Pogson, J. T. and MacGregor, R. K., "A Method of Increasing the Lateral Thermal Resistance of Multilayer Insulation Blankets," AIAA Paper 70-15, New York, 1970.

Performance of Disk-Gap-Band, Ringsail, and Cross Parachutes at Low Earth Altitudes

HAROLD N. MURROW* AND CLINTON V. ECKSTROM*
NASA Langley Research Center, Hampton, Va.

RECENT work at the NASA Langley Research Center concerning the use of parachutes in a low-density environment was aimed at studying decelerator operation at supersonic velocities and low dynamic pressures corresponding to expected conditions during terminal descent for landing on the planet Mars.[1] In order to obtain quantitative data concerning performance differences of lightweight geometrically porous parachutes between low- and high-density operations, 11 low-altitude flight tests were conducted at the Joint Parachute Test Facility at El Centro, Calif. It was hoped that correlation of the resulting data could lead to high-altitude performance predictions by conducting easier and more economical low-altitude tests. The test dynamic pressure q was adjusted upward for the low-altitude (high-density) tests in an attempt to obtain peak loadings similar to that experienced at high altitude. This Note discusses comparative high- and low-altitude performance characteristics of disk-gap-band (DGB), modified ringsail (RS), and cross parachute configurations which are shown in Fig. 1. The test payload configurations for both rocket-launched high-altitude tests and aircraft-dropped low-altitude tests were similar. Deployments for both test series were initiated by means of a mortar system,[2] whereby the parachute bridle, riser, and suspension lines deploy first, and a line stretch or snatch force occurs as the skirt portion of the canopy begins to leave the packing bag.

Results

Load-time histories from the high- and low-altitude tests of the DGB parachute are compared in Fig. 2a. The low-altitude test deployment was initiated at 10,300 ft and a q of 75 psf (a velocity of 300 fps), whereas the test at 140,000 ft was initiated at a q of only 11.6 psf (2030 fps). Although the low-altitude deployment was initiated at the higher q, the opening load was less because of the much larger decrease in q during the inflation sequence. For the high-altitude test,[3] q decreased very little during the inflation process, and the maximum loading came very near the time of first full inflation, although the equilibrium canopy loading W/C_DS

Presented as Paper 70-1164 at the AIAA Aerodynamic Deceleration Systems Conference, Dayton, Ohio, September 14–16, 1970; submitted October 2, 1970; revision received December 16, 1970.

* Aerospace Technologist. Member AIAA.